The following publication L. Xiao, S. Niu, M. Jiang and L. Dai, "Design and Analysis of a Resonant Induction Motor," in IEEE Transactions on Industrial Electronics, vol. 73, no. 2, pp. 1760-1769, Feb. 2026 is available at https://doi.org/10.1109/TIE.2025.3600523.

Design and Analysis of a Resonant Induction Motor

Longfei Xiao, Shuangxia Niu, *Senior member*, *IEEE*, Mingyuan Jiang, and Litao Dai, *Member*, *IEEE*

***Abstract*—Induction motors (IMs) with round and solid rotors are widely utilized in mining, water pumping, and agricultural applications due to their robustness, low cost, and minimal maintenance. However, their rated performance is often unsatisfactory, characterized by low torque and efficiency. This paper proposes a resonant induction motor (RIM) to explore the series resonant principle for enhancing IM performance at minimal cost. In contrast to prior designs requiring resonant capacitors occupying 70% of the EM active volume (stator/rotor windings and core), the proposed RIM reduces this to only 5% of the EM active volume. This is particularly relevant for round and solid rotor IMs with poor rated performance. Firstly, the motor's static parameters and the required resonant capacitors are analyzed and calculated using the equivalent circuit and the two-dimensional eddy current field finite element method (2D-EC-FEM). Subsequently, a RIM prototype is constructed to validate the theoretical analysis. Experimental results from the RIM prototype, which incorporates appropriate electromagnetic parameters and integrates resonant capacitors into the stator windings, demonstrate significant performance enhancements. Under the same voltage supply and rated conditions, the RIM achieves a higher power factor, greater maximum torque, and an improved torque-efficiency correlation compared to a conventional IM.**

***Index Terms*—EM, Enhanced Power Factor, FEM, Resonant Induction Motor, Resonant principle, T-type Circuit, and Torque-efficiency Correlation.**

I. Introduction

INDUCTION motors (IMs) are widely used in industrial and civil systems due to their ruggedness, high reliability, and cost-effectiveness. Their electromagnetic (EM) structure does not rely on rare earth permanent magnets, reducing manufacturing costs and improving durability [1]-[4]. This design allows IMs to operate in diverse environments, making them suitable for various applications.

Among these applications, IMs are extensively utilized in mining machinery [5], [6], such as conveyor belts and crushers, as well as in agriculture for driving water pumps and irrigation systems [7], [8]. They are available in a wide range of power ratings, from a few hundred watts (W) for smaller applications to several tens of kilowatts (kW) for industrial tasks. This adaptability makes them a preferred choice in both traditional and emerging sectors.

As the industry increasingly focuses on sustainability, IMs show great growth potential in the future motor market [4]-[10]. However, achieving optimal performance in terms of torque, efficiency, and power factor remains a daunting challenge. Conventional IM with wound or solid rotors often make trade-offs between these parameters, limiting their effectiveness in high-performance applications [11]-[13].

A key challenge in motor design is to achieve the best torque-efficiency relationship while improving the power factor under rated operating conditions. Traditional designs make it difficult to make the best efficiency point appear at the maximum torque point in rated conditions, resulting in poor motor performance.

In recent years, researchers have investigated resonant inductive coupling as a potential solution to this challenge. This principle has gained widespread attention in the development of advanced wireless power transfer systems as rotary transformers [14]-[16], where compensation capacitors are integrated at both the transmitting and receiving ends to achieve precise tuning, thereby improving power transfer efficiency while minimizing power supply requirements.

Applying the magnetic resonance principle to IMs presents more complex challenges in terms of the EM and mechanical design of the motor, especially in the calculation of parameters such as winding inductance and resonant capacitance. Researches in [17]-[19] adopted a resonant induction motor (RIM) with air core, which completely eliminated the effects of iron losses and simplified the calculation of winding parameters and resonant capacitance. However, these designs required oversized capacitors (3×1653 uf, 3 pole pairs, 150 Hz, synchronization speed of stator field is 3000 rpm, slip s is 0.3, rotor speed is 2100 rpm) whose volume was 6703 cm^3 , approximately 70% of the motor's EM active volume (windings and cores). Previous designs also led to the efficiency as low as 23% and torque significantly lower than that of conventional IMs. In addition, the RIM design which is proposed in [20]-[22] must operate at high speeds and frequencies, typically above 14,000 rpm, to achieve general motor performance. However, their applicability is limited, as most IMs operate within a speed range of 1000 to 3,000 rpm. Within this range, the design cannot function properly.

Manuscript received 17 December 2024; revised 08 February 2025 and 01 July 2025; accepted 05 August 2025. *(Corresponding author: Shuangxia Niu.)*

Longfei Xiao, Shuangxia Niu, Mingyuan Jiang and Litao Dai are with the Department of Electrical and Electronic Engineering, The Hong Kong Polytechnic University, Hong Kong 999077, China (e-mail: longfei.xiao@connect.polyu.hk; eesxniu@polyu.edu.hk; m.y.jiang@polyu.edu.hk; litao.dai@polyu.edu.hk).

Limited previous studies have focused on RIM designs, with only a few researchers proposing directions, topological structures that require large-size capacitors (mf) and excessively high frequencies (kHz), making them challenging to implement and lacking practical application value. In contrast, this paper proposes a RIM design that significantly improves practicality by using a small capacitor with a volume of only 60.48 cm³, which is only 5% of the motor's EM active volume and is consistent with the typical operating speed range of most motors (less than 3,000 rpm).

In addition, the method for calculating and adjusting the static parameters of motors and resonant capacitors is discussed based on the two-dimensional eddy current field finite element method (2D-EC-FEM) and a T-type equivalent circuit. To enable the application of the resonant principle, the RIM prototype incorporates a magnetic core stator and a wound rotor without slip rings, facilitating straightforward calculations and adjustments of static parameters. By exploiting resonance, higher performance metrics are achieved, including maximum torque near the peak efficiency point, while maintaining a power factor that exceeds that of conventional induction motors (IMs). A potential approach is proposed to enhance the performance characteristics of electric machines and effectively addresses the inherent trade-offs in electric machine design.

In Section-II, the configuration of RIM is introduced. In Section-III, the calculation of motor structure, resonant capacitance and static parameters is discussed by combining T-type equivalent and 2D-EC-FEM methods; in the Section-IV, the EM performance of variable resonant capacitor RIM and original IM is studied based on FEM method; in the Section-V, a prototype is built based on the analysis results, and experiments are carried out to verify the feasibility of the proposed ideas; finally, this paper is summarized in the Section-VI.

II. Configuration of RIM

Fig. 1 illustrates the topology of the proposed series RIM. The fundamental motivation for the proposed RIM is to utilize magnetic resonant coupling in a unified approach for electromechanical energy conversion systems. Additionally, the magnetic core, in conjunction with appropriate slot and winding arrangements, is designed to optimize the motor's equivalent reactance, avoiding the issue of excessively large size for CBB capacitors (metallized polypropylene film capacitors) at the required operating frequency, which could pose challenges in practical applications.

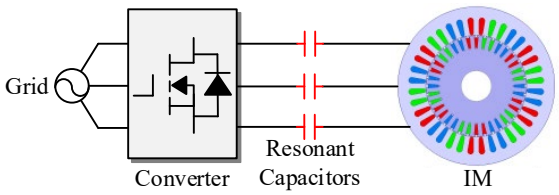

Fig. 1. The configuration of series RIM system.

Fig. 2. Dimensions of a 10.6 μF CBB capacitor.

CBB capacitor's volume and specifications are shown in Fig. 2 and TABLE I [23], [24]. The selection of CBB film capacitors is primarily due to their non-polarity, low capacitance drop, low loss, and high voltage withstand capability, making them particularly well-suited for resonant applications. To align with other research initiatives, the rated design specifications for this motor are presented in TABLE II.

TABLE I
RATED SPECIFICATIONS OF THE CBB CAPACITORS

Features	Symbol	Unit	Value
Voltage rating	U_N	V	63-2000
Rated capacitance	C_R	uF	0.001-10
Operating temperature	*Temp*	℃	-40~+80
Dissipation factor	*DF*	/	≤0.001(1KHz)
Equivalent series resistance	*ESR*	Ω	<0.1
Expected life	*MTBF*	hours	60000

TABLE II
RATED SPECIFICATIONS OF THE DESIGNED RIM

Features	Symbol	Unit	Value
Rated voltage	U_{line}	V	125
Rated frequency	f	Hz	150
Rated slip range	s	/	0.03-0.07
Actual rotor speed	n_r	rpm	2910-2790
Synchronization speed	n_s	rpm	3000
Calculated Capacitance	C_1	uF	Around 18

The proposed design offers several key merits:

1) Improved power factor: The integration of magnetic resonant coupling enhances the power factor, resulting in improved system efficiency.
2) Optimal torque-efficiency correlation: The design facilitates the alignment of the optimal efficiency point and maximum torque point within a favorable and rated slip range, ensuring enhanced performance in practical applications.
3) Reduced capacitor size for RIM: Compared to previous research that typically employs capacitors in the mF range, the proposed motor utilizes capacitors in the μF range, enabling effective operation within conventional power frequency ranges commonly used in market products. This reduction in size helps minimize the bulkiness of components, facilitating easier integration into existing systems.

III. PARAMETER ANALYSIS OF RIM

Analysis and modification of motor parameters are the initial and fundamental steps for RIM design procedure, as shown in Fig. 3. A three-phase RIM is a nonlinear and complex EM system where motor parameters fluctuate with changes in voltage, frequency, and current. Therefore, accurate estimation methods for these parameters are essential to effectively design the EM structure of the RIM and ensure optimal compatibility with the resonant capacitor.

This chapter introduces a method to calculate the high-precision equivalent static parameters of the motor using a T-type equivalent circuit model combined with the 2D-FEM. It details the process for calculating and adjusting the resonant capacitor C_1, highlighting important considerations for selecting the resonant point and determining the corresponding inductance values. The calculated parameters are then compared with experimental results.

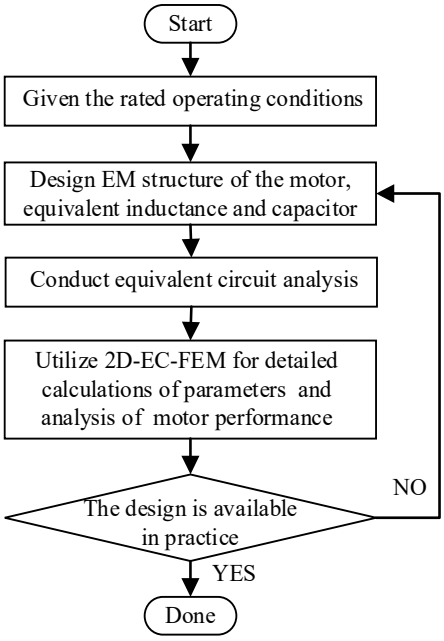

Fig. 3. The design procedure of RIM

A. T-type Equivalent Circuit Analysis

For motors, the equivalent circuit model is one of the most effective tools for characterizing the EM phenomena of motors. It can not only characterize the EM phenomena of motors through circuit parameters, but also simplify complex EM interactions into circuit problems, allowing designers to intuitively analyze the characteristics of motors.

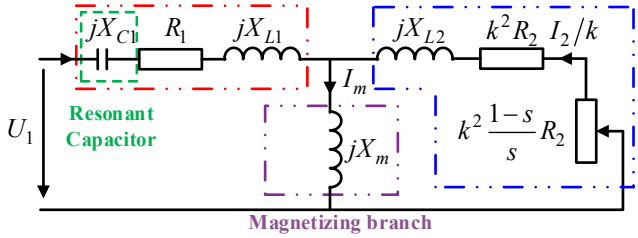

Fig. 4. Single phase equivalent circuit of the proposed RIM.

The equivalent circuit of RIM is shown in Fig. 4, which contains three branches: stator, rotor and magnetization.

The magnetizing branch focus on magnetizing reactance X_m, with the magnetizing resistance omitted for simplification. The magnetizing branch impedance Z_m is expressed as below:

$$Z_m = jX_m = j\omega_1 kL_m \tag{1}$$

where ω_1 represents the angular frequency of drive current, k is the turns ratio of stator to rotor windings and L_m denotes magnetizing inductance.

The stator branch consists of resonant capacitive reactance X_{C1}, phase resistance R_1 and leakage inductive reactance X_{L1}. The stator branch impedance Z_1 is defined as:

$$Z_1 = jX_{C1} + R_1 + jX_{L1} = -j\frac{1}{\omega_1 C_1} + R_1 + j\omega_1 L_1 \tag{2}$$

where C_1 and L_1 are the external resonant capacitance and stator phase leakage inductance, respectively.

In the rotor branch, referred to the stator side, X_{L2} denotes the rotor leakage inductive reactance, while k^2R_2 represents the rotor phase winding resistance. Additionally, the term $k^2\frac{1-s}{s}R_2$ illustrates the effect of slip s on the rotor resistance, which is crucial for understanding motor performance under varying load conditions. Slip s and rotor branch impedance Z_2 are described as follow:

$$s = \frac{(n_s - n_r)}{n_s} \tag{3}$$

where, n_S reflects the synchronous speed of the magnetic field and n_r represents the actual rotor speed.

$$\begin{aligned} Z_2 &= jX_{L2} + k^2R_2 + \frac{k^2R_2(1-s)}{s} \\ &= j\omega_1 L_2 + k^2R_2 + \frac{k^2R_2(1-s)}{s} \end{aligned} \tag{4}$$

where, L_2 is the rotor phase leakage inductance.

The equivalent impedance of RIM as viewed from the stator terminal can be determined from equations (5) to (8), which provide insights into its real and imaginary components , as detailed in equations (7) and (8).

$$Z_{eq} = Z_1 + Z_2 // Z_m \tag{5}$$

$$\begin{cases} O_1 = L_1 + kL_m \\ O_2 = L_2 + kL_m \\ O_3 = L_1L_2 + k(L_1 + L_2)L_m \end{cases} \tag{6}$$

$$\mathrm{Re}[Z_{eq}] = R_1 + \frac{sR_2\omega_1^2 L_m^2 k^4}{R_2^2k^4 + s^2\omega_1^2 O_2^2} \tag{7}$$

$$\mathrm{Im}[Z_{eq}] = -\frac{1}{\omega_1 C_1} + L_1\omega_1 + \frac{\omega_1 L_m R_2^2 k^5 + kL_2L_mO_2s^2\omega_1^3}{R_2^2k^4 + O_2^2s^2\omega_1^2} \tag{8}$$

According to equation (8), the series resonant capacitor required to offset the equivalent inductive reactance of the RIM can be expressed as equation (9).

$$C_1 = \frac{R_2^2 k^4 + {O_2}^2 s^2 \omega_1^2}{O_1 R_2^2 \omega_1^2 k^4 + O_2 O_3 s^2 \omega_1^4} \tag{9}$$

The power factor of RIM is calculated as equations (10) and (11).

$$\begin{cases} O_4 = R_2^2 k^4 + s^2 \left(X_2 + X_m\right)^2 \\ O_5 = R_1^2 + \left(X_{L1} + X_{C1} + X_m\right)^2 \\ O_6 = R_1^2 \left(X_{L2} + X_m\right)^2 \\ O_7 = \left[\left(X_{L1} + X_{C1}\right) X_2 + \left(X_{L1} + X_{C1} + X_{L2}\right) X_m\right]^2 \end{cases} \tag{10}$$

$$\begin{aligned} PF &= \mathrm{Re}[Z_{eq}] \Big/ \left|Z_{eq}\right| \\ &= \frac{R_1 O_4 + s R_2 X_m^2 k^2}{\sqrt{O_4}\sqrt{2 s R_1 R_2 X_m^2 k^2 + O_5 R_2^2 k^4 + \left[O_6 + O_7\right] s^2}} \end{aligned} \tag{11}$$

The maximum torque T_{max} and corresponding slip S_{pk} of conventional IM and RIM (under a sine voltage source) are shown in equations (12) [25] and (13) [17], respectively.

$$\begin{cases} a_1 = 1 + \dfrac{X_{L1}}{X_m} \\ T_{max\_IM} = \dfrac{m p U_1^2}{2 a_1 \omega_1 \left[R_1 + \sqrt{R_1^2 + \left(X_{L1} + a_1 X_{L2}\right)^2}\right]} \\ s_{pk\_IM} = \dfrac{a_1 R_2}{\sqrt{R_1^2 + \left(X_{L1} + a_1 X_{L2}\right)^2}} \end{cases} \tag{12}$$

$$\begin{cases} T_{max\_RIM} = \dfrac{m p U_1^2}{4 \omega_1 R_1 k^2} \\ s_{pk\_RIM} = \dfrac{R_1 R_2 X_m^2 k^2 + R_1 \sqrt{R_2^2 \left(X_m^4 - 4 O_6\right) k^4}}{2 O_6} \end{cases} \tag{13}$$

where, m is the phase number and p is the number of pole pairs.

According to equation (12), for IM, under a constant voltage and frequency, an increase in leakage inductance L_1, L_2 will reduce the maximum torque and also decrease the power factor [25]. Furthermore, the rotor resistance R_2 of IMs with solid or wound rotors tends to be relatively high and is difficult to modify in design, which often results in the peak torque occurring at lower speeds (high slip s).

For RIM, based on the equation (13), resonant capacitance can reduce the impact of leakage inductance to some extent and more easily control the area where the maximum torque occurs. Additionally, by varying the applied capacitance C_1, the speed range where maximum torque occurs can be adjusted, allowing T_{max} at higher speeds (lower slip s) and a higher power factor, thereby enhancing motor performance.

This phase resonant capacitor is greatly influenced by motor inductance L_1, L_2, L_m, the slip s, driven frequency f and so on. As f increases or s decreases, the required capacitance value for resonance diminishes. Conversely, when the inductance and frequency is too low or s is relatively high, the required capacitance value can increase by several tens or even hundreds of times. In addition, the resonance point is best to occur at a suitable frequency and a smaller slip rate s (closer to the synchronous speed) to ensure that the motor speed is within a reasonable range and has a higher operating efficiency.

To obtain the value of C_1, it is very important to predetermine static parameters of L_1, L_2, and L_m of one general IM without capacitance. If relying solely on the T-equivalent circuit, a completed prototype and a set of experiments [26]-[29] are required. The measurement process is quite complex, as outlined below:

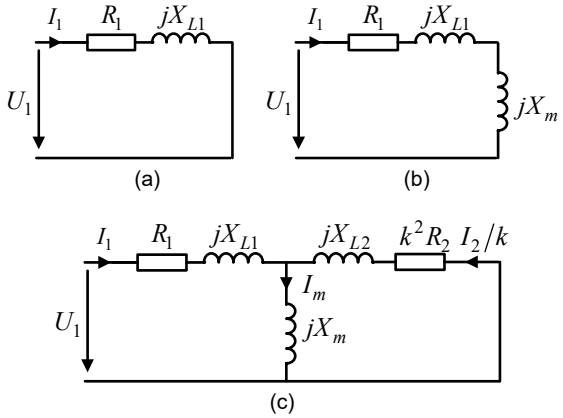

Fig. 5. Equivalent circuits for testing parameters of IM without capacitance. (a) Three-phase low-voltage non-rotor test. (b) Synchronous test. (c) Blocked rotor test.

1) Three-phase low-voltage non-rotor test [26],[27]: Stator parameter L_1 can be determined by conducting a three-phase low-voltage test on the stator windings in the absence of the rotor. This method eliminates the influence of the rotor and accounts for the mutual inductance among stator phase windings. Its equivalent circuit is illustrated in Fig. 5 (a).
2) Synchronous test [28],[29]: To accurately measure the magnetizing parameter L_m, a synchronous test is conducted by using a driving motor to bring the rotor of the protype to synchronous speed. At this condition, the slip s=0, causing the rotor circuit to behave as an open circuit, as shown in Fig. 5 (b).
3) Blocked rotor test [28],[29]: Following the completion of the first two experiments, the parameter L_2 of the rotor branch can be determined through a locked rotor test. In this test, the rotor speed n_r=0 and s=1. The equivalent circuit is shown in Fig. 5 (c).

The use of T-equivalent circuits allows for effective analysis of motor operation, however, it requires precise data of the equivalent circuit. To achieve the desired parameters and minimize measurement costs, these static parameters should be accurately calculated during the early design phase of the motor using 2D-EC-FEM.

B. 2D-EC-FEM Parameter Calculations and Experimental Verification

In the research, the authors use 2D EC-FEM to calculate the static parameters and analyze the performance characteristics of the RIM. Unlike transient field FEM (TF-FEM) [30], which relies on time-consuming iterative calculations in the time domain, EC-FEM operates in the frequency domain using a "direct solution method" [31],[32]. EC-FEM allows the field solution to be obtained in a single step, enabling fast and accurate calculations of the RIM [33]-[35].

When the motor is supplied with a specific power source, the three-phase magnetic flux linkage matrices in the stator and rotor are given by equation (15) and (16):

$$I_{1B} = I_{1C} = -0.5 I_{1A} \tag{14}$$

$$\begin{bmatrix} \psi_A \\ \psi_B \\ \psi_C \end{bmatrix} = \begin{bmatrix} L_{AA} & M_{AB} & M_{AC} \\ M_{BA} & L_{BB} & M_{BC} \\ M_{CA} & M_{CB} & L_{CC} \end{bmatrix} \begin{bmatrix} I_{1A} \\ I_{1B} \\ I_{1C} \end{bmatrix} \tag{15}$$

where Ψ_A represents the flux linkage of phase A in the stator winding, L_{AA} denotes the self-inductance of phase A, and M_{AB} , M_{AC}, etc., represent mutual inductance between stator three-phase windings.

$$\begin{bmatrix} \psi_a \\ \psi_b \\ \psi_c \end{bmatrix} = \begin{bmatrix} M_{Aa} & M_{Ba} & M_{Ca} \\ M_{Ab} & M_{Bb} & M_{Cb} \\ M_{Ac} & M_{Bc} & M_{Cc} \end{bmatrix} \begin{bmatrix} I_{1A} \\ I_{1B} \\ I_{1C} \end{bmatrix} \tag{16}$$

where Ψ_a denotes the flux linkage of phase a in the rotor winding, and M_{Aa} , M_{Ab}, etc., are mutual inductance between stator and rotor windings.

Based on the inherent symmetry of the winding configuration and the uniform characteristics of three phases, the mutual inductance relationship can be expressed as:

$$\begin{cases} M_{Aa} = M_{Bb} = M_{Cc} \\ M_{Ab} = M_{Bc} = M_{Ca} \\ M_{Ac} = M_{Cb} = M_{Ba} \end{cases} \tag{17}$$

According to (16) and (17), L_m is derived as (18). When transformed to the stator side, L_1 and L_2 are shown as (19) and (20).

$$L_m = \frac{|\psi|}{|I_1|} = \begin{pmatrix} M_{Aa}^2 + M_{Ab}^2 + M_{Ac}^2 - M_{Aa}M_{Ab} \\ -M_{Ab}M_{Ac} - M_{Ac}M_{Aa} \end{pmatrix}^{1/2} \tag{18}$$

$$L_1 = L_{AA} - M_{AB} - kL_m \tag{19}$$

$$L_2 = k^2 (L_{aa} - L_{ab}) - kL_m \tag{20}$$

Combining equations (6) and (8) from section A with the inductance values obtained from the 2D-EC-FEM calculations allows for the determination of the required resonant capacitance for an established motor product. However, common motors available on the market that utilize resonant principles often require significantly larger non-polarized CBB capacitors.

Therefore, a critical consideration in the design process is how to minimize the size of the CBB capacitor while ensuring its rated performance.

TABLE III
DESIGN FEATURES OF THE DESIGNED RIM

Features	Symbol	Unit	Value
Stator Outer Diameter	D_{S1}	mm	125
Stator Inner Diameter	D_{S2}	mm	80.5
Rotor Outer Diameter	D_{R2}	mm	79.5
Length	l	mm	70
Stator Slots	W_1	/	36
Rotor Slots	W_2	/	36
Turns Ratio of Stator to Rotor	k	/	1
Winding Turns	N	/	40
Pole pairs	p	/	3

TABLE IV
COMPARISON OF 2D-EC-FEM SIMULATION RESULTS AND EXPERIMENTAL MEASUREMENTS

Equivalent circuit inductance	Symbol	Unit	FEM	Measured
Stator leakage inductance	L_1	mH	5.06	5.53
Rotor leakage inductance	L_2	mH	5.15	5.59
Magnetizing inductance	L_m	mH	61.1	56.7

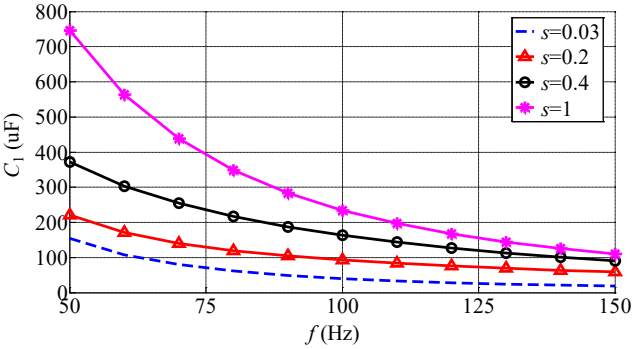

Fig. 6. Resonant capacitor under different frequency and slip.

TABLE V
RESONANT CAPACITANCE

s \ f	50 (Hz)	100 (Hz)	150 (Hz)
0.01	153.38 uF	38.48 uF	17.20 uF
0.03	154.82 uF	39.91 uF	18.62 uF
0.07	161.93 uF	46.78 uF	25.11 uF
0.2	220.31 uF	92.90 uF	58.68 uF
0.4	371.61 uF	163.43 uF	90.12 uF
1.0	745.54 uF	234.33 uF	109.70 uF

This mainly involves the appropriate adjustment and design of the equivalent inductance of the designed motor, which depends on the motor structure, number of winding turns, rated voltage, rated frequency and slip ratio s of the motor. In order to keep the volume of the resonant capacitor within the appropriate range, the following factors must be considered:

1) Resonant point: The resonant point should be chosen at a lower slip (s=0.03−0.07). Although selecting the resonant point at startup (s=1) is possible, it may lead to an excessively large capacitor and high instantaneous current, posing significant risks.

2) Balance between winding turns and rated voltage: Increasing the number of winding turns can effectively enhance the inductance and reduce the required capacitor volume. However, this will also increase the necessary rated voltage and resistance. Additionally, the resonant capacitance also has a voltage rating limit, which must be maintained within a safe range.
3) Constraints on resistance and inductance: It is crucial to ensure that both resistance and inductance do not exceed acceptable levels. Excessively high resistance inductance can lead to increased losses and negatively impact control performance.
4) Rated frequency: Increasing the rated frequency can reduce the required capacitance, but the speed range of the motor and other practical factors must be considered.

Considering the above factors, the dimensional structure of the designed RIM is presented in TABLE III. TABLE IV shows the 2D-EC-FEM simulation results and the prototype experimental data. The difference between the two is within 10%, which confirms the effectiveness of the simulation model for the static analysis and calculation of resonant capacitors. The resonant capacitor C_1 under varying frequency f and slip s is partially detailed in Fig. 6 and TABLE V.

IV. Electromagnetic Performance of RIM

Here, the results of the performance analysis of the RIM at 150 Hz and 125 V line voltage using 2D-EC-FEM simulation are presented. It evaluates the effects of varying resonant capacitors C_1 on motor torque, stator phase current, power factor, loss, and efficiency. For medium and low power RIMs, the operating regime can be divided into four different intervals, as shown in TABLE VI.

TABLE VI
Operational States of Medium and Small Power RIMs

Region	Slip s
Rated range	[0.03, 0.07]
Extend range	(0.07, 0.1]
Non-standard range	(0.1, 1)
Startup	1

The rated operating range, characterized by constant voltage and frequency regime, is the core of this paper's discussion.

A. EM Torque, Current and Loss

Fig. 7 compares the flux distribution of the IM and RIM (with varying capacitors) at 125 V, s=0.03 and f=150 Hz, and the time is 0. As C_1 approaches the resonant value from equation (9) under these conditions，the overall magnetic flux density B is significantly improved.

For RIMs, the rapid variation of current near the resonance point may lead to dynamic changes in the effective magnetic permeability u_{r2} of the rotor silicon steel sheets. These changes can result in variations in the local magnetic flux density B, leading to increased iron loss, torque and power factor variations. The empirical formula for u_{r2} is given by:

$$u_{r2} = u_r - a/s \tag{21}$$

where u_r is the relative magnetic permeability (ranging from 5000 to 8000), and a is the correction factor (ranging from 45 to 55).

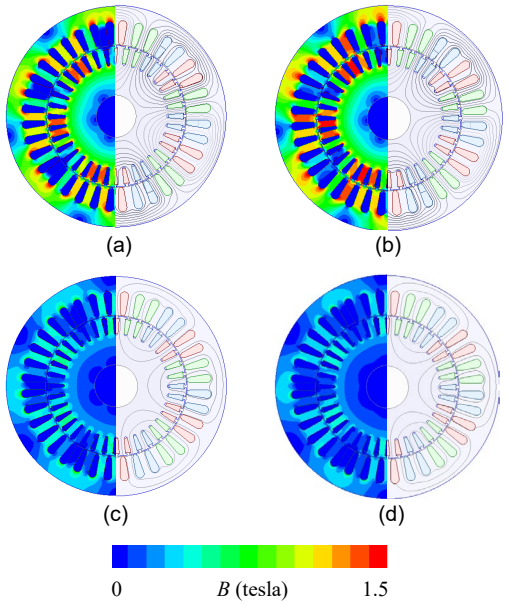

Fig. 7. Flux distribution of RIM and IM. (a) RIM with 15.6 uF. (b) RIM with 25.11 uF. (c) RIM with 107.9 uF. (d) IM.

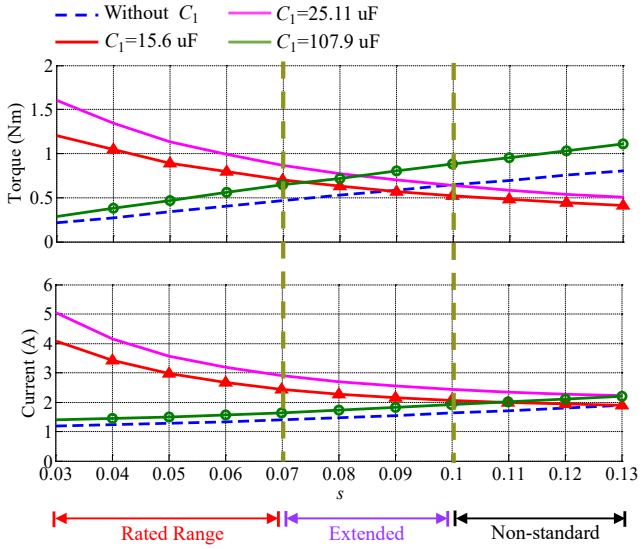

Fig. 8. FEM results of torque and stator phase current in the RIM under different capacitors at 125 V and 150 Hz.

Torque and current are presented in Fig. 8 and TABLE VII. For instance, within the rated range, the RIM with capacitance between 15.6 and 25.11 μF allows for higher current delivery, resulting in maximum torque that is 3 to 4 times greater than that of the IM. Fig. 9 and TABLE VIII present the loss and efficiency of the RIM and IM at 125 V and 150 Hz.

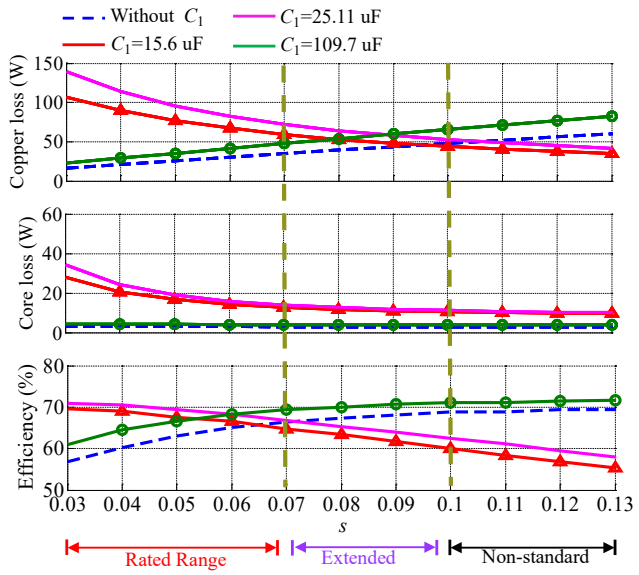

Fig. 9. FEM results of loss and efficiency in the RIM under different capacitors at 125 V and 150 Hz.

TABLE VII
FEM RESULTS OF TORQUE AND PHASE CURRENT IN THE RIM WITHIN THE RATED RANGE AT 125 V AND 150 HZ

Within Rated Range (s=0.03-0.07)			
Capacitor	Max Torque	Current	Slip
C_1 (uF)	T_{max} (Nm)	I (A)	s
15.6	1.206	4.082	0.03
25.11	1.601	5.05	0.03
109.7	0.646	1.64	0.07
Without	0.47	1.4	0.07

TABLE VIII
FEM RESULTS OF LOSS AND EFFICIENCY IN THE RIM WITHIN THE RATED RANGE AT 125 V AND 150 HZ

Within Rated Range (s=0.03-0.07)				
Capacitor	Copper loss	Core loss	Max Efficiency	Slip
C_1 (uF)	P_R (W)	P_c (W)	η (%)	s
15.6	106.87	27.8	69.54	0.03
25.11	139.7	34.3	70.96	0.03
109.7	50.10	4.03	69.48	0.07
Without	34.82	2.94	66.38	0.07

Although there are many factors that affect the iron loss, under constant voltage and frequency and normal temperature rise, the iron loss is mainly related to the magnetic flux density of the core. From Fig. 8 and Fig. 9, it can be observed that when the motor enters the rated operating range , current and the iron loss of RIM with corresponding resonant capacitance increases rapidly as the inductive reactance decreases.

In terms of efficiency, although the RIM exhibits higher losses compared to the IM within the rated slip range (s=0.03-0.07), the RIM demonstrates significantly higher torque. Therefore, by selecting an appropriate resonant capacitor, the efficiency of the RIM can be no lower than, or even exceed, that of the IM, particularly within a specific slip range.

B. Power Factor

The role of the stator series capacitor in this research is to compensate for the equivalent inductive reactance of the T-type equivalent circuit in the RIM, thereby realizing a theoretically pure resistance circuit. This configuration can make the power factor of the motor improved under specific s and f.

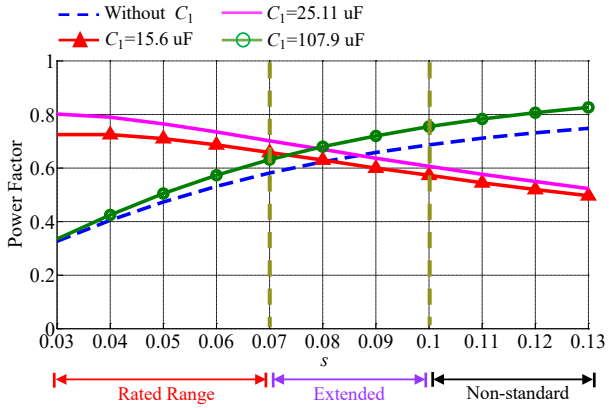

Fig. 10. FEM results of power factor in the RIM under different capacitors at 125 V and 150 Hz.

TABLE IX
FEM RESULTS OF POWER FACTOR IN THE RIM WITHIN THE RATED RANGE AT 125 V AND 150 HZ

Within Rated Rang (s=0.03-0.07)		
Capacitor	Max Power Factor	Slip
C_1 (uF)	PF_{max}	s
15.6	0.723	0.03
25.11	0.801	0.03
109.7	0.630	0.07
Without	0.581	0.07

Some curves and data are presented in Fig. 10 and TABLE IX. At 150 Hz, with s from 0.01 to 1, the theoretical capacitance required for complete compensation is between 17.2 and 109.7 μF (refer to TABLE V). In the rated operating range (s = 0.03 to 0.07), the required capacitance is 18.62 to 25.11 μF. Although capacitance exceeding 109.7 μF can also improve the power factor, it is inadvisable to exceed this limit due to safety and practicality concerns. Ideally, optimal operating conditions should be achieved in the high-speed range (i.e., when s is relatively small); thus, capacitance slightly below 17.2 μF such as 15.6 μF is also considered viable.

V. EXPERIMENTAL VERIFICATION

In order to verify the feasibility of the proposed topology, a RIM prototype is made according to the parameters in TABLE III. The internal structure is detailed in Fig. 11. Each stator phase winding is connected in series with CBB capacitor of 15.6 uF. The test platform for the prototype is demonstrated in Fig. 12, which mainly comprises dynamometer, inverter, power analyzer, master computer, etc.

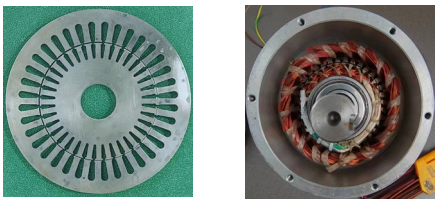

(a) (b)

(c)

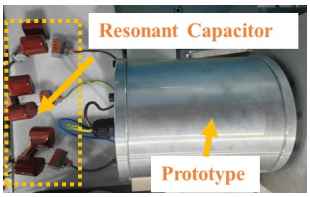

(d)

Fig. 11. Structure of the protype. (a) Silicon steel sheets. (b) Assembly. (c) A wound rotor with short circuit. (d) The prototype RIM with series resonant capacitors.

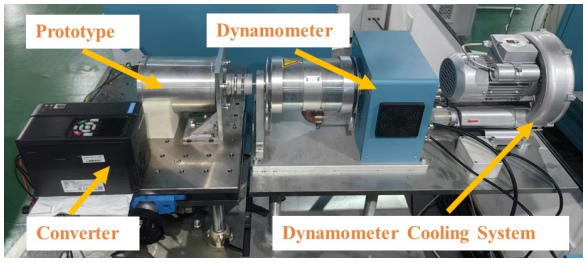

Fig. 12. Test platform.

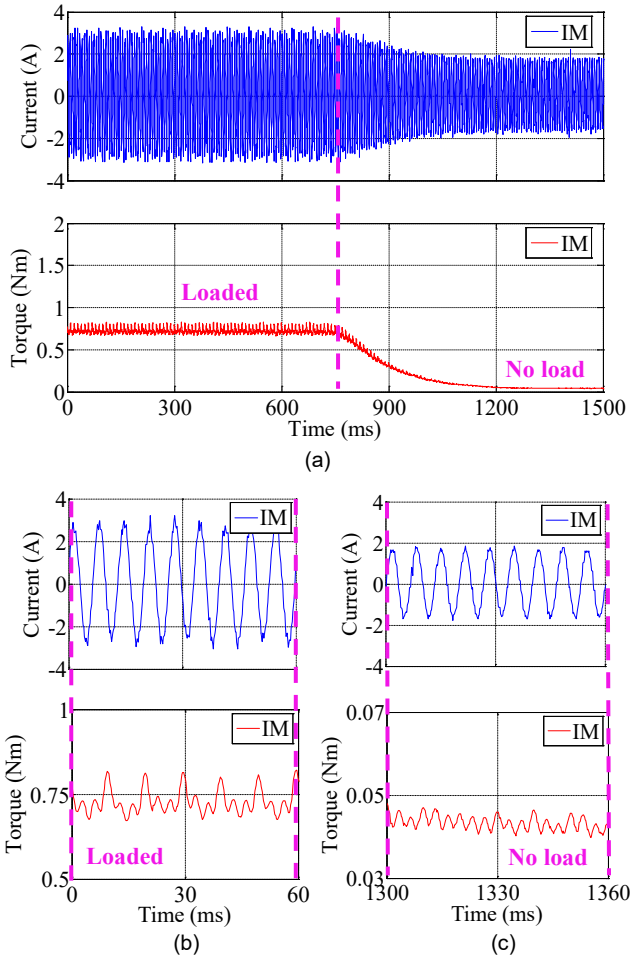

Fig. 13. Tested phase current and torque of IM. (a) The whole process. (b) Loaded. (c) No load.

In this study, both IM and the RIM were tested using the same inverter, with a set rated voltage of 125 V and a frequency of 150 Hz. Fig. 13 illustrates the current and torque variation of the IM transitioning from a loaded state to an unloaded state.

As shown in Fig. 14 and TABLE X, the RIM (150 Hz, 125 V, 15.6 uF) whose resonant point is around s = 0.04 exhibits a current amplitude increase from 1.47A (pre-resonance) to 3.32 A (post-resonance), 80% in torque output (0.51 Nm to 0.92 Nm) and a 0.17 power factor improvement (0.43 to 0.60).

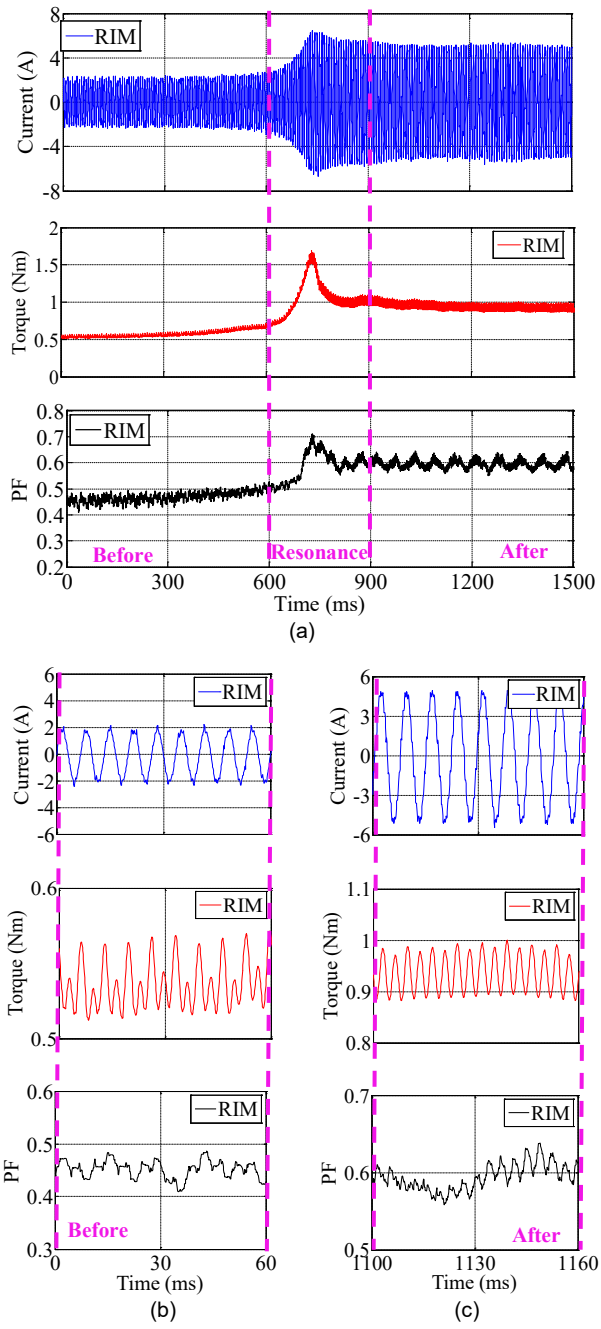

Fig. 14. Tested phase current and torque of RIM with 15.6 μF. (a) The whole process. (b) Before resonance. (c) After resonance.

TABLE X
PERFORMANCE COMPARISON OF RIM BEFORE AND AFTER RESONANCE WITH 15.6 UF AT 125 V AND 150 HZ

Parameters	Symbol	Before resonance	After resonance
Torque	T (Nm)	0.51	0.92
Current	I (A)	1.47	3.42
Power factor	PF	0.43	0.6

Fig. 15 and TABLE XI present a comparative analysis of test results between RIM and IM. RIMs have a "hard characteristic" and show better speed regulation under load. The speed remains stable over their rated operating range. IMs with wound/solid rotor motors have a "soft characteristic" and show poor speed regulation. Their speed is highly load dependent, and even a slight increase in load torque over their operating range will cause their speed to drop significantly and in proportion to the load torque.

TABLE XI
TEST RESULTS OF RIM AND IM AT 125 V AND 150 HZ

Within Rated Range (s=0.03-0.07)					
Motor	Torque	Current	Power factor	Eff	Slip
Type	T (Nm)	I (A)	PF	η (%)	s
IM	0.166	1.189	0.361	54.39	**0.03-0.04**
RIM	**0.914**	**3.50**	**0.601**	**62.76**	
IM	0.237	1.247	0.431	61.23	**0.04-0.05**
RIM	**0.863**	**3.47**	**0.568**	**63.11**	
IM	0.385	1.39	0.545	68.53	**0.05-0.07**
RIM	**0.778**	**3.01**	**0.567**	**61.87**	

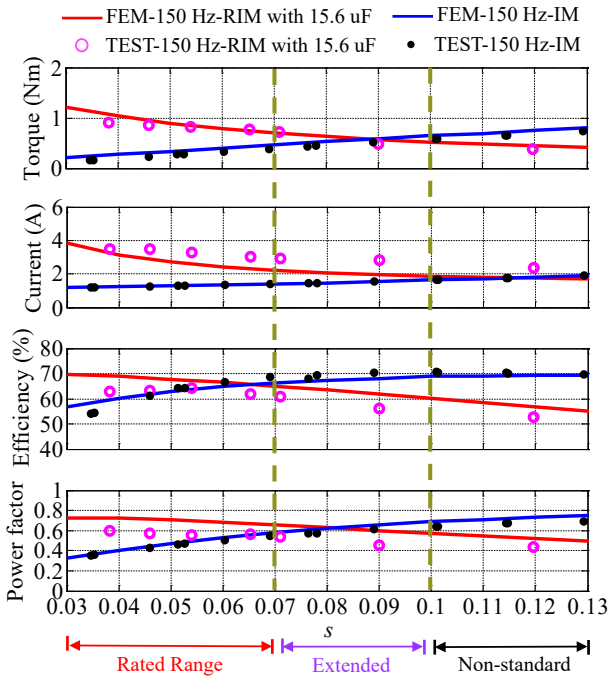

Fig. 15. Test and FEM comparison of RIM and IM at 125V and 150 Hz.

When the slip rate s is in the range of 0.03 to 0.07 (2910~2790 rpm), the comprehensive performance of RIM is better than that of IM, especially in the range of s=0.03 to 0.04, the torque of RIM is 5.51 times that of IM, the power factor is 0.24 higher, and the efficiency is improved by 8.37%. The test results verify that RIM can obtain better torque-efficiency correlation, power factor, and operating performance.

Although there are differences in power factor and performance compared to the simulation results, these can be attributed to the flowing factors:

1) Impact of dynamic parameters: The system may be more sensitive to changes in dynamic parameters, resulting in differences in the calculation results.
2) Manufacturing tolerances and assembly errors: Imperfections during the manufacturing process, such as deviations in rotor or stator dimensions, misalignment of components, or uneven air gaps, can affect motor performance.

Authors believe that improving the quality of silicon steel sheets, enhancing manufacturing precision, and reducing winding errors can enhance motor performance.

VI. CONCLUSION

This research investigates the design of RIM and analyzes its performance characteristics through finite element analysis and T-type equivalent circuit modeling. The accuracy of static parameter calculations, such as stator and rotor leakage inductance and magnetizing inductance, is verified by experiments conducted on the designed RIM prototype. The experimental results demonstrate that the RIM can significantly improve the torque-efficiency relationship compared to the conventional IMs. Within the rated slip range of s=0.03~0.05 (2910~2850 rpm), the RIM achieves substantial improvements in both torque and power factor. These "harder characteristics" make RIM particularly suitable for demanding applications such as mining machines in dusty places, where better torque-efficiency relationship and the ability to maintain speed under a certain load range are important.

This paper underscores the potential of RIM designs to enhance motor performance under critical operational conditions. RIM demonstrates a better torque-efficiency correlation with both the maximum torque point and the optimal efficiency point located near the rated point. Furthermore, the RIM prototype exhibits a torque that is 5.51 times greater than that of IM and a power factor improvement of 0.24 within the slip range of s=0.03~0.04 at 125 V and 150 Hz. The paper also identifies key areas for future research, including refining dynamic parameter modeling and exploring advanced design methodologies to fully exploit the benefits of resonant principles in RIM applications.

REFERENCES

[1] B. Podmiljšak *et al*., "The Future of Permanent-Magnet-Based Electric Motors: How Will Rare Earths Affect Electrification? " *Materials* 2024, *17*, 848.

[2] K. Baba, Y. Hiroshige, and T. Nemoto. "Rare-earth magnet recycling." *Hitachi Rev* 62.8 (2013): 452-455.

[3] F. J. T. E. Ferreira, A. M. Silva, V. P. B. Aguiar, R. S. T. Pontes, E. C. Quispe and A. T. de Almeida, "Overview of Retrofitting Options in Induction Motors to Improve Their Efficiency and Reliability," *2018 IEEE International Conference on Environment and Electrical Engineering and 2018 IEEE Industrial and Commercial Power Systems Europe (EEEIC / I&CPS Europe)*, Palermo, Italy, 2018, pp. 1-12.

[4] M. Toulan, A. Nafeh, and S. Arafa, "Improvement of Induction Motors Reliability in Fertilizers Plants Using IOT and Enterprise Resource

Planning", *2024 International Telecommunications Conference (ITC-Egypt)*, pp.487-492, 2024.
[5] S. G, W. M, P. S, and K. P, “Issues of Exploitation of Induction Motors in the Course of Underground Mining Operations,” *Archives of Mining Sciences*, vol. 62, no. 3, pp. 579–596, Sep. 2017.
[6] K. W, “How Do Induction Motors Perform Under Extreme Load Conditions in Mining?” *IEC Motores*. [Online]. Available: https://iecmotores.com/induction-motors-mining-performance/.
[7] M. A. Vitorino and M. B. R. Correa, "High performance photovoltaic pumping system using induction motor", *Proc. Brazilian Power Electron. Conf.*, pp. 797-804, 2009.
[8] K. W, “Why Are Induction Motors the Most Reliable Choice for Agricultural Water Pumps?” *IEC Motores.* [Online]. Available: https://iecmotores.com/induction-motors-agricultural-water-pumps/.
[9] V. Goman *et al*., "Comparative study of induction motors of IE2 IE3 and IE4 efficiency classes in pump applications taking into account CO2 emission intensity", *Applied Sciences*, vol. 10, no. 23, pp. 8536, 2020.
[10] I. Kaekbirdina and R. Khazieva, "Research on Highly Efficient Electric Motors with Increased Power Factor," *2023 Dynamics of Systems, Mechanisms and Machines (Dynamics)*, Omsk, Russian Federation, 2023, pp. 1-6.
[11] D. Zhang, J. Zhang, S. Wang, W. Peng, J. Yi and X. Wu, "Electromagnetic Design and Optimization of High-Speed Solid-Rotor Induction Motor," *2023 IEEE 6th Student Conference on Electric Machines and Systems (SCEMS)*, HuZhou, China, 2023, pp. 1-6.
[12] D. T. McGuiness, M. O. Gulbahce and D. A. Kocabas, "A performance comparison of different rotor types for high-speed induction motors," *2015 9th International Conference on Electrical and Electronics Engineering (ELECO)*, Bursa, Turkey, 2015, pp. 584-589.
[13] M. Aoyama and T. Noguchi, "Squirrel-Cage Type Induction Machine Utilizing Space Harmonics for Secondary Excitation with Concentrated Winding Stator," *2018 21st International Conference on Electrical Machines and Systems (ICEMS)*, Jeju, Korea (South), 2018, pp. 514-519.
[14] T. Raminosoa, R. H. Wiles and J. Wilkins, "Novel Rotary Transformer Topology With Improved Power Transfer Capability for High-Speed Applications," in *IEEE Transactions on Industry Applications*, vol. 56, no. 1, pp. 277-286, Jan.-Feb. 2020.
[15] B. Song, S. Shi, S. Cui, S. Dong, Q. Zhang and S. Ren, "Wireless Power Transmission Excitation Systems for Electrically Excited Motors: Comparison of Magnetic Coupler Topologies," *2024 IEEE 10th International Power Electronics and Motion Control Conference (IPEMC2024-ECCE Asia)*, Chengdu, China, 2024, pp. 5009-5013.
[16] K. Li, Y. Liu, X. Sun, X. Tian, G. Lei, "Applications of Wireless Power Transfer System in Motors: A Review", *IEEE Access*, vol.12, pp.80590-80606, 2024.
[17] Z. Jin, *et al*., "Air-Cored Resonant Induction Machines: Comparison of Capacitor Tuning Criteria and Experimental Validation," in *IEEE Transactions on Industry Applications*, vol. 57, no. 4, pp. 3595-3606, July-Aug. 2021
[18] Z. Jin *et al*., "Design Optimization Procedure of Air-Cored Resonant Induction Machines," *2021 IEEE Energy Conversion Congress and Exposition (ECCE)*, Vancouver, BC, Canada, 2021, pp. 4089-4096
[19] Z. Jin *et al*., "A Fast 3-D Winding Inductance Estimation Method for Air-Cored Resonant Induction Machines," in *IEEE Transactions on Industry Applications*, vol. 58, no. 5, pp. 6125-6135, Sept.-Oct. 2022.
[20] A. Abuallah, Y. Komi, R. Deodhar and C. Umemura, "Hybrid Resonant Induction Machine for High-Speed Applications," IECON 2021 – 47th Annual Conference of the IEEE Industrial Electronics Society, Toronto, ON, Canada, 2021, pp. 1-6.
[21] A. Abduallah, Y. Komi and S. Hirose, "Resonant and Hybrid Resonant Induction Machine Performance Comparison for High-Speed Applications," *IECON 2023- 49th Annual Conference of the IEEE Industrial Electronics Society*, Singapore, Singapore, 2023, pp. 1-6.
[22] B. J. Ebot and Y. Fuiimoto, "A General Framework for the Analysis and Design of a Wireless Resonant Motor," *2019 IEEE International Electric Machines & Drives Conference (IEMDC)*, San Diego, CA, USA, 2019, pp. 1966-1970.
[23] H. Li *et al.*, “Modeling of ESR in metallized film capacitors and its implication on pulse handling capability,” *Microelectronics Reliability*, vol. 55, no. 7, pp. 1046–1053, Jun. 2015.
[24] "CBB81 Capacitors," KEC Capacitor, [Online]. Available: https://www.kscapacitor.com/products/cbb81-capacitors.html
[25] D. R. Wu, *Electric Machinery*, 1st ed., ser. 2, ch. 19, pp. 294, China: Water Resources and Electric Power Press, Nov. 1979.
[26] H. Chen and C. Bi, "Influence of Driving State on Parameters of Three-phase Induction Motor," *2021 IEEE 4th International Electrical and Energy Conference (CIEEC)*, Wuhan, China, 2021, pp. 1-6.
[27] H. Chen and C. Bi, " An effective method for determination and characteristic analysis of induction motor parameters", *IET Electric Power Applications.* 2022, vol 16, issue 5, pp. 605 – 615.
[28] "IEEE Draft Standard Test Procedure for Polyphase Induction Motors and Generators," in *IEEE P112/D5*, vol., no., pp.1-110, 1 Jan. 2015.
[29] D. Bhowmick, M. Manna and S. K. Chowdhury, "Improved equivalent circuit parameter estimation of induction motor using H-G diagram and PSO," *2017 IEEE Calcutta Conference (CALCON)*, Kolkata, India, 2017, pp. 443-447.
[30] Maxwell help, ANSYS, Inc, Canonsburg, PA 15317, USA, vol.15, pp 36, 2020.
[31] CompleteMaxwell2D_V14, ANSYS, Inc, Canonsburg, PA 15317, USA, Vol.1, pp 8, 2011.
[32] H. Igarashi and T. Honma, "On convergence of ICCG applied to finite-element equation for quasi-static fields," in *IEEE Transactions on Magnetics*, vol. 38, no. 2, pp. 565-568, March 2002.
[33] O. Chiver, L. Neamt, C. Barz and C. Costea, "Frequency domain numerical analysis of rotor cage induction motor," *2014 International Conference and Exposition on Electrical and Power Engineering (EPE)*, Iasi, Romania, 2014, pp. 327-331.
[34] Maxwell help, ANSYS, Inc, Canonsburg, PA 15317, USA, vol.27, pp 20, 2020.
[35] G. -J. Park, B. Son, S. Seo, J. -H. Lee, Y. -J. Kim and S. -Y. Jung, "Compensation Strategy of the Numerical Analysis in Frequency Domain on Induction Motor Considering Magnetic Flux Saturation," in *IEEE Transactions on Magnetics*, vol. 54, no. 3, pp. 1-4, March 2018.

Longfei Xiao received his B.Eng. degree in electrical engineering from Shanghai DianJi University, China, in 2016, and the M.Eng degree in electrical engineering from University of Shanghai for Science and Technology, China, in 2020. He had worked as a motor designer at two technology companies: Fortior Technology Co., Ltd. in Shenzhen, China, from 2020 to 2021, and Shanghai Mingzhi Electric Co., Ltd. in Shanghai, China, from 2021 to 2023. He is currently a Ph.D. student with the Department of Electrical and Electronic Engineering, The Hong Kong Polytechnic University, Hong Kong. His main research interests include the EM analysis and design of induction machines.

Shuangxia Niu received the B.Sc. and M.Sc. degrees in electrical engineering from Tianjin University, China, in 2002 and 2005, respectively, and the Ph.D. degree from The University of Hong Kong, Hong Kong, in 2009. She is currently a professor with the Department of Electrical and Electronic Engineering, The Hong Kong Polytechnic University. She authored or coauthored more than 200 papers in leading journals. Prof. Niu is currently an Associate Editor for the IEEE Journal of Emerging and Selected Topics in Power Electronics. She is Distinguish Lecturer of IEEE Vehicular Technology Society.

Mingyuan Jiang received the B.Eng. degree in electrical engineering and automation from Shanghai Maritime University, Shanghai, China, in 2020, and the M.Sc. and Ph.D. degrees in electrical engineering from The Hong Kong Polytechnic University, Hong Kong, China, in 2021 and 2024. He is currently a Research Assistant Professor in the Department of Electrical and Electronic Engineering, The Hong Kong Polytechnic University. His primary research focuses on the design, optimization, and control of electric machines, electric vehicles, and power generation.

Litao Dai (Member, IEEE) was born in Changsha, China, in 1993. He received the B.S. degree in mathematics from Harbin University of Commerce, Harbin, China, in 2015, and Ph.D. degree in electrical engineering from Hunan University, Changsha, China, in 2023.

He is currently working as a Postdoctoral Fellow with the Department of Electrical and Electronic Engineering, The Hong Kong Polytechnic University, Hong Kong, SAR, China.